JOURNAL OF GUIDANCE, CONTROL, AND DYNAMICS
Vol. 17, No. 4, July–August 1994

# Test Bench for Rotorcraft Hover Control

Martin F. Weilenmann* and Hans P. Geering†
*ETH Swiss Federal Institute of Technology, CH-8092 Zurich, Switzerland*

**This paper describes an indoor stand for a computer-controlled model helicopter. This stand was built to verify modern multivariable controller algorithms in real-world tests rather than in simulations. A commercial radio-controlled helicopter (not a scale model) is mounted on a mechanical structure allowing 6-degree of freedom flight conditions in a 2-m cube. The symmetrical geometry of the frame reduces its physical influence on the rotorcraft to be equivalent to a concentrated mass near the center of gravity. Including the dynamics of the driving motor and some unsteady aspects of the aerodynamics, an unstable 18th order mathematical model results. In addition, the radio controller causes a significant time delay. For this system, several control algorithms have been applied [channelwise proportional differential (PD) controller used for system identification, Linear Quadratic Gaussian/Loop Transfer Recovery (LQG/LTR) approaches, modal controller]. The quality of the test results and some aspects of design problems are described and compared in the second part of the paper.**

## Nomenclature

$A_M$ = collective pitch angle, rad
$A_T$ = collective tail rotor pitch angle, rad
$A_{1s}$ = longitudinal cyclic stick input, rad
$a_{1p}$ = lateral flapping angle of Bell-Hiller stabilizer bar, rad
$B_{1s}$ = lateral cyclic stick input, rad
$b_{1p}$ = longitudinal flapping angle of Bell-Hiller stabilizer bar, rad
$G_t$ = transfer function of Padé approximation
$T_t$ = time delay, s
$p$ = roll rate, rad/s
$q$ = pitch rate, rad/s
$r$ = yaw rate, rad/s
$u_l$ = state of motor controller, V
$u_h$ = forward velocity, m/s
$v_l$ = induced velocity, m/s
$v_{Tl}$ = induced velocity tail rotor, m/s
$v_h$ = sideward velocity, m/s
$w_h$ = vertical velocity, m/s
$\Delta\Omega$ = rotor speed difference to nominal, rad/s
$\Theta$ = pitch angle, rad
$\Phi$ = roll angle, rad
$\Psi$ = yaw angle, rad
$\zeta$ = vertical inertial position, m
$\eta$ = sideward inertial position, m
$\xi$ = forward inertial position, m

*Subscript*

$d$ = reference signal for the controller

## I. Introduction

WITH the beginning of the era of robust control in the mid-1980s, modern multivariable control algorithms became "practicable;" i.e., multivariable controllers dealing with output feedback with guaranteed stability margins became feasible for a large number of linear plants. Our laboratory was searching for a "real" multi-input multi-output (MIMO) plant of laboratory size to test the performance of controllers and to compare different algorithms in the "real world." A system was sought that had considerable interaction between the different inputs and outputs in order to avoid treating several single-input single-output (SISO) problems side by side. Because test and simulation for a perfectly modeled plant are identical, our plant was not to be perfectly modeled.

Eventually, we decided on a radio-controlled (RC) helicopter with a rotor diameter of 1.4 m. This model helicopter is not to scale to a specific helicopter type; however, the Reynolds number is in the range of light two-bladed types. This rotorcraft was mounted on top of a mechanical frame that allowed free motion in a 2-m cube. The geometry of this frame originates from the delta robot.[1] This frame is used for safety, and to measure the position and attitude of the rotorcraft by potentiometers. With the concept of the overall installation shown in Fig. 1, automated position control, as discussed in this paper, or flying with human pilots is possible.

A large part of this paper is dedicated to a detailed description of the testbed and its mathematical model because free-flight conditions are achieved. Additionally, several controller designs are presented to show their performance on this bench and the differences between simulations and real-world tests.

A description of the construction and dynamics of the frame is given in Sect. II. In Section III, some aspects and details of the modeling of the rotorcraft are presented. An overview of the mathematical modeling is given in Sect. IV. In Sect. V, we discuss some problems encountered and compare the results of different controllers designed. Section VI is a summary of the experience with the test bench.

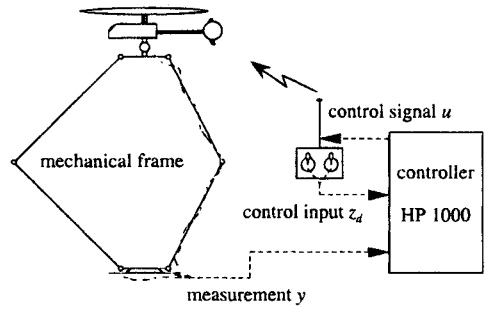


**Fig. 1 Concept of the test bench.**

Received June 1, 1993; presented as Paper 93-3853 at the AIAA Guidance, Navigation, and Control Conference, Monterey, CA, Aug. 9–11, 1993; revision received Sept. 21, 1993; accepted for publication Oct. 27, 1993. 

*Research Assistant, Measurement and Control Laboratory. Student Member AIAA.

†Professor of Control and Mechatronics, Measurement and Control Laboratory. Senior Member AIAA.

## II. Description of Frame

### A. Geometry

The ground plate is a symmetric triangle. At every corner of the ground plate, a 1.91-m rod is attached by a cylindrical joint. The axes of these joints are normal to the centerline of the triangle. The 2.14-m upper rods are attached to the lower rods by Cardan joints with 2 degrees of freedom (DOF). The same joints connect these rods to the top triangular plate (Fig. 2).

This geometry has the following features: The upper plate is always parallel to the ground and cannot rotate around the vertical axis. The inertial position of the upper plate ($\xi$, $\eta$, $\zeta$ are used here to avoid conflicts with the signals $x$, $y$, $z$ of control theory) is given by the angles between the lower rods and the ground plate.

The frame is exposed to the following loads. Prior to takeoff, it carries the weight of the rotorcraft. In flight, it is carried by the helicopter, and only the dynamic forces of its own structure are present. When the helicopter reaches the limits given by the frame, the load suffered by the structure is in the range of the weight of the helicopter. The maximal possible loads, thus, are in the range of the weight of the rotorcraft; i.e., 4 kg. Therefore, the material selected for the construction of the rods may be light, so our helicopter has to carry about 3.8 kg of the frame. This is a normal payload for an RC helicopter.

The RC helicopter itself is linked to the center of the upper plate by a 3-DOF joint (ball joint) to allow free-flight conditions. This joint must be attached to the helicopter near its center of gravity to minimize torques acting on the upper plate causing flexural vibrations.

### B. Kinematics

Because the frame consists of three closed kinematical chains, common multibody approaches for kinematics do not apply directly. Nevertheless, because of the symmetry of the structure, the inertial position and velocity of the upper plate can be calculated if the three angles at the bottom are given. Each corner of the upper plate lies on the surface of a sphere with a known center (top of the lower rod) and a constant radius (length of the upper rod). (Pertinent equations are contained in Appendix A.)

The complete kinematics; i.e., the translation and rotation of every rigid body in the system as a function of the motion of the upper plate, can only be given by implicit equations because of the complexity of the problem. These equations must be solved numerically.

### C. Dynamics

In this application, we are interested in what forces the helicopter "sees" of the frame it has to carry. We discuss some aspects of the static forces first and look at the dynamic forces separately.

As we move the frame out of the symmetrical position wherein the upper plate is exactly above the lower one, both the value and the direction of the static force necessary to carry the frame change. Because the horizontal part of that force does not exist in free flight, it must be minimized. By analogy, the vertical force will be constant and as small as possible because the rotorcraft must carry the frame.

In order to reach these goals, we evaluated various geometries of longitudinal and torsion springs for attachment to the bottom, middle, or top joints. Because the middle and top joints have 2-DOF, it was not possible to find a spring with satisfactory behavior for those locations.

The concept presented in Fig. 3, with springs at the bottom joints for all three legs, showed the best performance. The value of the vertical force is decreased by 30% with such springs. The vertical force is constant within 2% over 2.5 m of height, and it does not change by a horizontal offset for a diameter range of 2.4 m. The horizontal force remains below 0.6% of the weight the helicopter finally carries.

As mentioned in Section B, the complete kinematics of this structure cannot be given analytically. Even for a case in which the upper plate moves with a constant speed, it is not possible to compute the translational and rotational velocities and accelerations of the different rods explicitly. Thus, the exact dynamic forces the helicopter experiences cannot be calculated.

However, that calculation can be replaced by the following practical tests. The upper plate is attached to the inertial system with stiff springs. When that system is made to oscillate freely, two conditions must be met for the frame to be considered a point mass. First, the oscillation must keep its initial direction; i.e., only forces in the direction of motion may occur. Our structure fulfills this condition perfectly. Second, when that test is performed at various points anywhere in the work space, the eigenfrequency must be identical at all points. The value of the inertial mass calculated from the eigenfrequencies measured remains constant within 1% for all horizontal motions and within 0.2% for all vertical motions. The comparison of these local linear measurements with the dynamics calculated for some special cases; e.g., symmetrical geometry, shows a good coincidence for the velocity range of interest.

Thus, we conclude that, to the helicopter, the frame appears to be a concentrated mass at the location of the ball joint. The physical effects of that virtual mass, however, have different values for gravitation mass, 3.8 kg, vertical inertia, 3.6 kg, and horizontal inertia, 3.9 kg.

The lowest flexible modes of the rods are near one-third of the nominal rotor speed. Because the frame is connected to the helicopter by a spherical joint, they are not excited significantly.

## III. Description of the Helicopter

The rotorcraft used on this test bench is a commercial RC model (Graupner Avant Garde) with a two-bladed rotor of 1.4-m diam. The main rotor is assisted by a Bell-Hiller stabilizer bar, which consists of two small rotor blades mounted on the rotor shaft at a right angle to the main blades and linked to those mechanically (Fig. 4). Because of their large inertia relative to their aerodynamic surface, they react slowly to control inputs and to pitch and roll disturbances. This damping effect facilitates

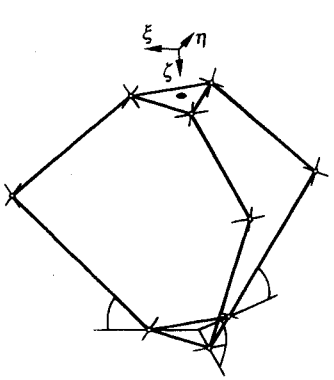


Fig. 2 Frame.

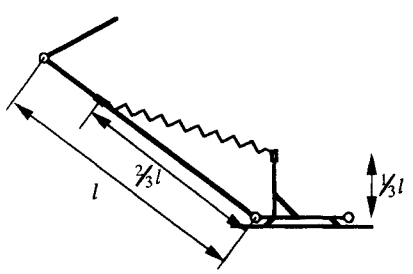


Fig. 3 Spring layout.

the guiding of the RC helicopter by a human pilot. The tail rotor is also two-bladed and is linked to the main rotor by a 4:1 transmission.

The rotorcraft in the laboratory is modified from its original design in that it is driven by a dc motor to avoid exhaust gases and reduce noise. An operational amplifier on the ground supplies the power to this motor. The overall weight of 7.9 kg for the helicopter and the frame requires a power of 0.8 kW and a rotor speed of 1560 rpm. As real helicopters are, this craft is controlled by four inputs.

The vertical position is controlled with collective pitch angle. The tail rotor pitch angle controls the yawing angle. The forward inertial position and the pitch angle are controlled by the longitudinal cyclic stick input, while the lateral cyclic stick input controls the roll angle and sideward inertial position.

## IV. Mathematical Modeling

### A. Physical Background

Dynamic modeling of helicopters is well described in the literature.[2-5] Basically, the modeling of this test bench helicopter follows those concepts. The small size of this rotorcraft causes certain details to be somewhat different, however.

The modeling starts with the classical rigid-body equations. For position control of the helicopter, 12 state variables result. Because the flight speed in any direction is so small, we assume that the aerodynamic forces acting on the body of the helicopter are negligible. Therefore, only gravitation and the different forces and moments from the main and tail rotors need to be modeled.

As is usual for two-bladed rotors, there are no lead-lag joints. Because of the high stiffness of the blades compared to those of normal helicopters, the first-order flapping equations hold very precisely. The time constant of the flapping motion of the main rotor is more than one decade above that of the motions of the helicopter body, and thus may be neglected. Taking into account the flapping motion of the Bell-Hiller stabilizer bar, which "slows down" the dynamics as mentioned in Section III, yields two more state variables to our model. While the aerodynamic forces are modeled as described by Johnson[3] or Prouty[4] for no-twist blades with the approximation of constant induced velocity over the rotor disk, the experience of flight tests showed certain differences. Not only the absolute value of induced velocity varies in vertical flight conditions, but there is a time delay in the downwash reacting to abrupt pitch changes. According to Prouty[4] (pp. 115ff.), this effect is negligible for normal helicopters. For our small craft, however, the typical time constants are smaller. The downwash time constants for the main and tail rotors, thus, add two more state variables to the model.

Finally, the dynamics of the dc motor fitted with a proportional integral (PI) controller for constant speed must be taken into account as well. Thus, we finally have a nonlinear model with 18 states that holds for hover and flight with slow velocities in any direction.

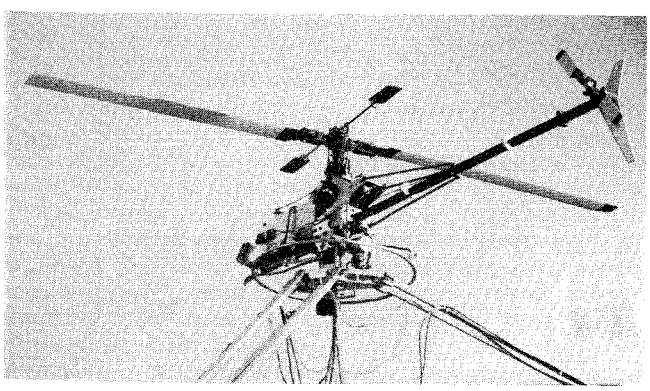

**Fig. 4 Photo of helicopter, main rotor with Bell-Hiller stabilizer bar.**

### B. Linear Model

For the controller design, this mathematical model was linearized around the hover position. This leads to the state space description

$$\begin{aligned} \dot{\boldsymbol{x}} &= \mathbf{A}\boldsymbol{x} + \mathbf{B}\boldsymbol{u} && \boldsymbol{x} \in \boldsymbol{R}^{18},\ \boldsymbol{u} \in \boldsymbol{R}^4 \\ \boldsymbol{y} &= \mathbf{C}_I\boldsymbol{x} && \boldsymbol{y} \in \boldsymbol{R}^6 \text{ measurement vector} \\ \boldsymbol{z} &= \mathbf{C}_{II}\boldsymbol{x} && \boldsymbol{z} \in \boldsymbol{R}^4 \text{ output vector } (z) \subset (y) \end{aligned} \tag{1}$$

The state vector $\boldsymbol{x}$ contains the following state variables:

$$\begin{aligned} \boldsymbol{x} = (&\xi\ \eta\ \zeta\ u_h\ v_h\ w_h\ \Phi\ \Theta\ \Psi \\ &p\ q\ r\ a_{1p}\ b_{1p}\ \Delta\Omega\ u_I\ v_I\ v_{TI})^T \end{aligned} \tag{2}$$

The input vector

$$\boldsymbol{u} = (A_{1s}\ B_{1s}\ A_M\ A_T)^T \tag{3}$$

The measurement vector $\boldsymbol{y}$ is a subset of the state vector $\boldsymbol{x}$

$$\boldsymbol{y} = (y_1, \ldots, y_6)^T = (\xi\ \eta\ \zeta\ \Phi\ \Theta\ \Psi)^T = \mathbf{C}_I\boldsymbol{x} \tag{4}$$

while the output vector $\boldsymbol{z}$ is a subset of the measurement vector $\boldsymbol{y}$

$$\boldsymbol{z} = (z_1, \ldots, z_4)^T = (\xi\ \eta\ \zeta\ \Psi)^T = \mathbf{C}_{II}\boldsymbol{x} \tag{5}$$

The numerical values of the matrices **A, B** are given in Appendix B. $\mathbf{C}_I$ and $\mathbf{C}_{II}$ follow from Eqs. (4) and (5).

### C. Subsystems

This linear system has the following characteristics. Obviously, the collective pitch of the main rotor causes lift and creates reaction torques. The reaction torque influences the yaw motion via the dynamics of the engine causing a strong coupling between the vertical motion and the yaw motion. This effect normally is compensated by a direct connection of the main collective to the tail collective signal, by gyro stabilizers, or both. These gyros are mechanical P or PD (proportional or proportional differential) controllers affecting the collective control of the tail rotor. Because of the motor dynamics, such controllers are limited to low bandwidths.

The motions in the horizontal plane; i.e., the dynamics of forward–backward and sideward motions with pitch and roll angles, are coupled physically by the main rotor. The geometry is chosen in such a way that forward and sideward motions are statically decoupled.

These two main parts of the system are connected by small couplings only. These parts have different typical velocities; i.e., different crossover frequencies. In addition, each part describes a different physical structure. Thus, it makes sense to design the controllers for two separate subsystems individually, using the experience of the two steps to then build an overall controller. The first subsystem describes the vertical and the yaw motions:

$$\begin{aligned} \boldsymbol{x}_1 &= (\zeta\ w_h\ \Psi\ r\ \Delta\Omega\ \ u_I\ v_I\ v_{TI})^T \\ \boldsymbol{u} &= (A_M\ A_T)^T, \qquad \boldsymbol{y}_1 = \boldsymbol{z}_1 = (\zeta\ \Psi)^T \end{aligned} \tag{6}$$

The second subsystem describes the dynamics between the longitudinal and the lateral cyclic inputs, the roll and pitch motions, and the forward and sideward movements.

$$\begin{aligned} \boldsymbol{x}_2 &= (\xi\ \eta\ u_h\ v_h\ \Phi\ \Theta\ p\ q\ a_{1_p}\ b_{1_p})^T \\ \boldsymbol{u}_2 &= (A_{1s}\ B_{1s})^T \end{aligned} \tag{7a}$$

$$z_2 = (\xi\ \eta)^T, \qquad y_2 = (\xi\ \eta\ \Phi\ \Theta)^T \tag{7b}$$

## V. Controller Design

### A. Special Plant Properties, Design Goals

Because the linear model of the helicopter contains two conjugate poles in the right-hand part of the complex plane and six poles at the origin, it is clearly unstable. Equations (4) and (5) show that the control vector $z$ is only a subset of the measurement vector $y$. The measurement vector $y$ consists of the three angles of attitude of the helicopter and of its inertial position. When the rotorcraft hovers, the pitch and roll angles are given by the trim condition, thus a reference signal would not be meaningful. The measurement of pitch and roll angles is nonetheless important, as discussed in Section V.C.2.

Transmission of the controller commands, via the multiplexing radio controller, takes 80 ms. This time delay must be taken into account for the design of fast controllers. It has been verified that a second order Padé approximation suffices here to model it:

$$G_t = (-s\ 2/T_t + 6/T_t^2)/(s^2 + s\ 4/T_t + 6/T_t^2) \tag{8}$$

$$\text{with} \quad T_t = 0.08$$

Adding this transfer function at every input of the system yields a total of 26 states for the overall system; i.e., 12 states for the first subsystem and 14 states for the second subsystem. With that approximation, the overall system has four nonminimum phase zeros. From this point on, the plant referred to is augmented by that Padé approximation.

The goal of the control design is a controller with 1) good disturbance rejection in the low-frequency band; and 2) a robustness margin given by the maximal sensitivity of 4 dB. The transfer function from the reference signal $z_d$ to the output signal $z$ should be close to diagonal; i.e., the coupling of the system is to be small.

In Section V.B., the design of a classic controller is presented. The design with Linear Quadratic Gaussian/Loop Transfer Recovery (LQG/LTR) algorithms is described in Section V.C. In Section V.D, modal approaches are presented, and in Section V.E, the results of the different designs are compared.

### B. Classical Controller

Some of the parameters needed for the mathematical model can be measured only in actual flight. Thus, we needed to fly the rotorcraft. Rather than flying with a human pilot to measure some parameters we decided to implement PD controllers in order to obtain representative results.

The controller for the horizontal $\xi$ and $\eta$ positions had to be cascaded around the controllers for pitch and roll angles (Fig. 5). Without the "inner" controller for pitch and roll angles, it is not possible to realize a stable loop. This structure was tuned for best disturbance rejection, which for PD controllers is the same as high gain or high bandwidth, respectively.

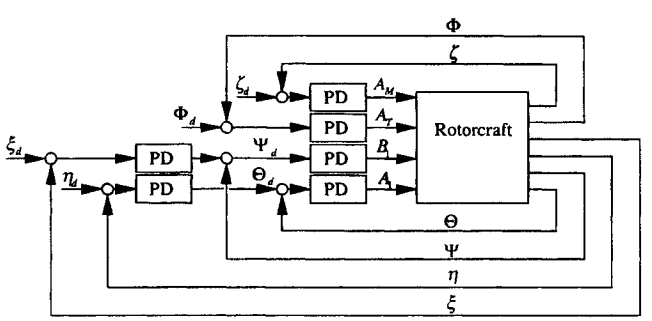


**Fig. 5 Cascaded PD controller.**

### C. LQG/LTR Controllers

As mentioned in Section IV.C., the helicopter may be separated into two subsystems with very little interaction. From the theoretical point of view, the problems presented by the two systems differ considerably.

#### 1. *First Subsystem*

The subsystem for vertical and yaw motions is of the order 8. The dominant eigenvalues of the two paths of this system differ by a factor of 5. The time constant of the interacting dynamics lies in-between. Matching the singular values of the system, as required in the classical LQG/LTR approach, does not make sense here because of the different nature of the two paths.

As stated above, the system is nonminimum phase. Considering that the maximal crossover frequency of interest (5-8 rad/s) is one-fourth of the value of the Padé approximation zero (37.5 rad/s), we can expect satisfactory robustness in the LTR step, nevertheless.

The design of a controller with a crossover frequency of between 5 and 8 rad/s and a robustness satisfying our requirements (Fig. 6) follows next. The measurement noise caused by the rotor vibrations and the digital realization of the controller are the reasons why the eigenvalues of the estimator in the LTR step cannot be pushed arbitrarily high. Nonetheless, the sensitivity convergence is good. The design parameters are given in Appendix C.

Although the closed-loop behavior with this controller is satisfactory, the input–output behavior is not. A step input causes the control signal $u$ to result in a short, high peak that saturates the servos. The time response of the system shows an overshoot of 50%.

As in classic controller design, such behavior is avoided by never leading the reference signal into any differentiating controller parts. In our case, therefore, the reference signal is led statically to the controller output (Fig. 7). With this feed-forward reference input, the peaks in $u$ are reduced by a factor

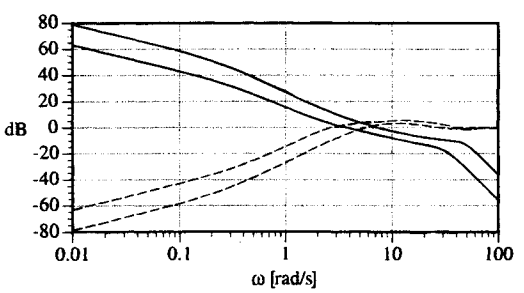


**Fig. 6 Singular values of the open-loop transfer function $L(j\omega)$ (solid line) and of the sensitivity function $S(j\omega)$ (dashed line) of the LQG/LTR design for the first subsystem.**

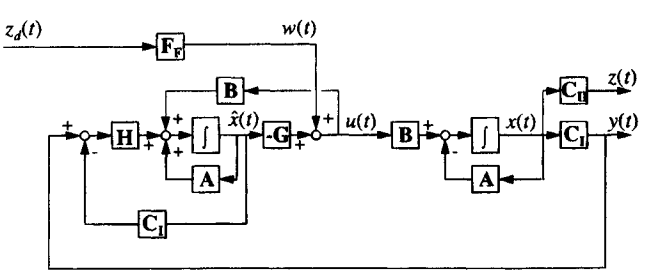


**Fig. 7 Block diagram for the system with feed-forward reference input.**

of 5, and overshooting is reduced to 10%. The prefilter matrix $F_F$ is calculated so that the transfer function of the closed-loop system from $z_d$ to $z$ becomes an identity matrix for $s = 0$. Thus, we prevent both static offset and static coupling.

Because the maximal absolute value of the nondiagonal transfer function matrix elements is less than −20 dB, the dynamic coupling also is satisfactorily small. This is confirmed by the simulation of a vertical step response where the yaw angle remains smaller than 2.5 deg. (Fig. 8). As the servo *velocities* are limited (i.e., $\dot{u}$), starting with Fig. 8, the reference signals are actually "ramp signals" of 0.7 s, which prevent saturation. This does not affect the interpretation, however.

*2. Second Subsystem*

This 10th-order subsystem describes the horizontal motion of the rotorcraft. There are two inputs and four measured signals: $\xi$ and $\eta$ positions; and roll and pitch angles. When prescribing the inertial position of the helicopter, the roll and pitch angles are "internal" signals. If we do not use the angle measurements for the controller design, however, the plant model receives two pairs of conjugate zeros lying on the imaginary axis.

As we found in the first subsystem, the standard design yields an unsatisfactory input–output behavior. Here, the step response overshoots by 60%. Using the same concept for the reference input as before leads to a much more damped behavior (Fig. 9a). This design fulfills the robustness specifications. The coupling in the second subsystem is less than −45 dB.

Figure 9b shows the measurement of the same step response in the real plant. The comparison of the simulation to the measurement results shows the following. The fast behaviors of the pitch angle look very similar. The fact that the two position signals, $\xi$, differ after two s is because of unmodeled, nonlinear effects of the unstationary airflow.

*3. Synthesis*

The combination of the design parameters of the two subsystems in one block diagonal parameter matrix yields a controller for the entire rotorcraft. Although the performance of this controller is similar to that of the two subsystem controllers running in parallel, the decoupling is improved.

### D. Modal Controllers

In controller design for rotorcraft, modal approaches are often used because the U.S. Department of Defense publishes aircraft handling specifications in frequencies and damping.[6,7] Controlling only the rotations of the helicopter (for human-piloted vehicles) leads to systems of order 6–8. Every path of the system is then of second or third order only. Thus, the eigenvalues have the same meaning as in the mass–spring–damper problem[8,9,10].

Because modal control does not guarantee robustness, however, it would be difficult to set the eigenvalues for a large system such as ours (as we control the position of the rotorcraft) in such a way that robustness and decoupling can both be achieved. We decided to use modal control for perfect decoupling following Lohmann[11] for completeness' sake. We attempted to leave the highest possible number of eigenvalues at the location of the Linear Quadratic Regulator (LQR) design described in Section V.C. With this approach, we attempted to retain most of the robustness achieved. Finally, an LTR observer was used similar to that detailed in Section V.C. Its exact design parameters have only a small influence on the overall performance.

In theory and simulation, the decoupling achieved with modal control is perfect. The measurements, however, show that in the real world, the decoupling is not better than that achieved with the LQG/LTR approach described in Section V.C. (see Fig. 10). This difference between the theoretically exact decoupling and the real-world measurements reflects the accuracy of the linear model for this nonlinear plant.

### E. Comparison of Control Laws

Performance results are shown in Table 1. High average crossover frequency and high static gain indicate good disturbance rejection. Satisfactory robustness is achieved with a maximum sensitivity below 4 dB. The quality of decoupling is given by the largest nondiagonal value of the transfer function from the reference $z_d$ to the output $z$.

As expected, the model-based controllers show a much better performance than the cascaded PD controller. Modal control

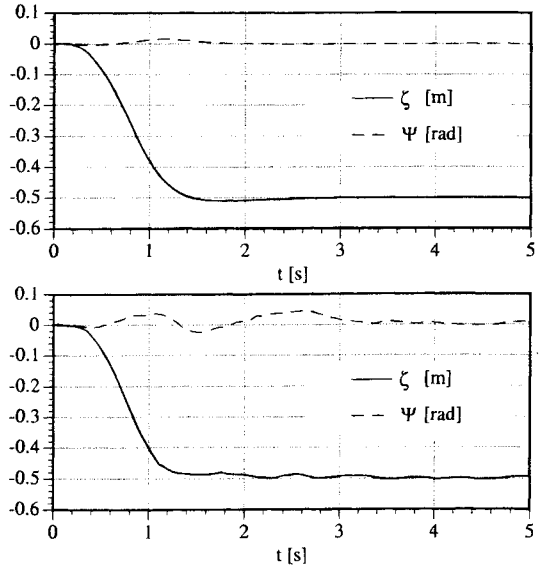


**Fig. 8 Simulation and measurement of vertical step response.**

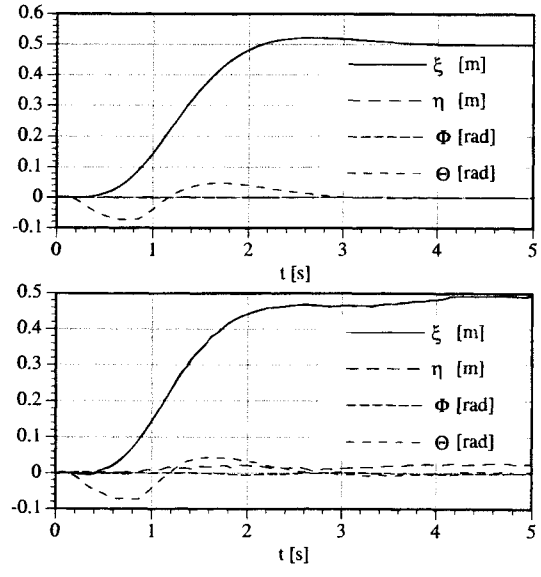


**Fig. 9 Simulation and measurement of forward step response for feed-forward reference input.**

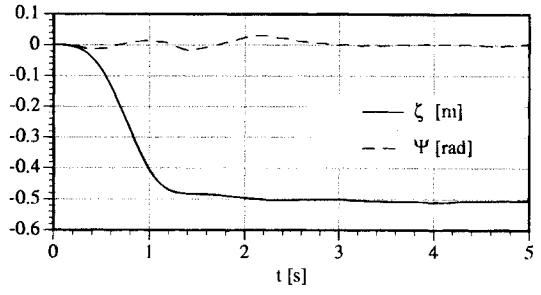


**Fig. 10 Measurement of vertical step response (modal controller).**

**Table 1 Summary of results**[a]

| Controller properties | PD controller | LQG/LTR controller, 1st subsystem | LQG/LTR controller, 2nd subsystem | LQG/LTR controller, full system | Modal controller, 1st subsystem | Modal controller, 2nd subsystem |
|---|---|---|---|---|---|---|
| Average crossover frequency, rad/s | 3.5 | 5.7 | 5.4 | 5.55 | 5.7 | 4.8 |
| Maximum sensitivity, dB | 7.1 | 4.2 | 3.8 | 4.2 | 5.2 | 12.5 |
| Maximum value of nondiagonal $G_{ij}$ | 1.09 | 0.0923 | 0.0057 | 0.0941 | 0 | 0 |
| Static gain, $\xi \rightarrow B_{1s}$ | −0.0252 | —— | −0.2703 | −0.2690 | —— | −0.0724 |
| $\eta \rightarrow A_{1s}$ | 0.0868 | — | 0.2897 | 0.2862 | — | 0.4574 |
| Static gain, $\zeta \rightarrow A_M$ | 0.0960 | 0.1190 | —— | 0.1189 | 0.0977 | —— |
| Static gain, $\Phi \rightarrow A_T$ | −0.2037 | −0.3021 | —— | −0.3061 | −0.2506 | —— |

[a]Values in this table are scaled by equations B3 and B4.

generally is useful only for small plants where each path is of 3rd or 4th order, at most. The perfect decoupling is useful only for plants where the linear mathematical model is a very close approximation over a large range of the state space.

The natural limit of robustness in the presence of nonminimum phase zeros, the so-called "waterbed effect" of Freudenberg and Looze,[12] indicates that for our requirements of 4 dB maximal sensitivity, the performance of the controller of Section V.B. is close to the "physical" limit.

## VI. Conclusions

This paper presents a laboratory-size test bench for indoor flying near hover under free-flight conditions. The frame allows precise and easy measurements of position and attitude that can be used for offline processing or feedback control. Thus, it is an interesting laboratory tool that permits flying by human pilots as well as by automated controllers.

The application of different controller designs for position control show the superiority of modern multivariable concepts over classic approaches. However, usually the "recipes" from control theory must be adapted to the problem, as shown by the feed-forward reference input used to improve the input/output behavior of the LQG/LTR design. In the presence of unmodelled dynamics, robust approaches perform better than do modal controllers.

## Appendix A: Transformation of the Frame Geometry

The transformation from the bottom angles of the frame to the inertial position of the upper plate is given here in Fortran 77 code. This code is optimized in speed; i.e., least possible number of trigonometric functions and multiplications.

```
C Inputs
C 11 =1.91 ! Length of lower rods
C 12 =2.14 ! Length of upper rods
C da =0.22 ! Distance of the bottom
C   and top joints to the center of the
C   triangular plates
C alphas (1..3) ! angles between lower
C   rods and floor
C Outputs
C xi, eta, zeta ! cartesian coordinates of
C   top plate
C Transformation of bottom joint angles
C   to inertial coordinates of the upper
C   plate (xi, eta, zeta)

  b1 =cos(alphas (2)) * 11 + da
  b2 =cos(alphas (3)) * 11 + da
  a1 =cos(alphas(1)) * 11 + da
  a2 =sin(alphas(1)) * 11
  a3 =−0.866025404 * b1 ! *SQRT(3)/2
  a4 =−0.5 * b1
  a5 =sin(alphas(2)) * 11
  a6 =0.866025404 * b2 ! *SRTQ(3)/2
  a7 =−0.5 * b2
  a8 =sin(alphas(3)) * 11
  b3 =a1 − a4
  b4 =a2 − a8
  b5 =a1 − a7
  b6 =a2 − a5
  b7 =a2*a2 + a1*a1
  b8 =−b7 + a5*a5 + a4*a4 + a3*a3
  b9 =−b7 + a8*a8 + a7*a7 + a6*a6
  a9 =2*(b3*b4 − b5*b6)
  a10 =b4*b8 − b6*b9
  a11 =2*(a3*b4 − a6*b6)
  a12 =2*(a6*b3 − a3*b5)
  a13 =a6*b8 − a3*b9
  a14 =a11*a11
  a15 =a9*a9 + a14
  a16 =2*(a10*a9 − a1*a14)
  a17 =−2.0*a14*a2
  a18 =a14*(b7 − 12*12) + a10*a10
  b10 =a12*a12
  b11 =a14*(b10 + a15)
  a19 =(a17*b10 + a11*(a12*a16 − 2.0*a13*a15))/b11
  a20 =(a18*b10 + a13*(a13*a15 − a12*a16))/ b11
  h1 =a19*a19 − 4.0 0*a20
  IF (h1 .LE. 0.0) THEN
    CALL Beep
    h1 =0.0
  END IF
  koordG(3) =(SQRT(h1) − a19) * 0.5
  koordG(2) =−(a13 − a11*koordG(3))/ a12
  h2 =(12*12) − (koordG(3) − & a2)*(koordG(3) −a2)
  − (koordG(2) −a1)*(koordG(2)−a1)
  IF (h2 .LE. 0.0) THEN
    CALL Beep
    h2 =0.0
  END IF
  koordG(1) =SQRT(h2)
  IF (alphas(3) .GT. alphas(2))
    & koordG(1) =−koordG(1)

C Displacing the center of the inertial
C system into the center of the workspace
  xi =−koordG(1)
  eta =koordG(2)
  zeta =−koordG(3) + 1.47 ! Offset of
       the center of the workspace
```

## Appendix B: State Space Matrices of the Mathematical Model

**A** =

Columns 1 thru 8

| | | | | | | | |
|---|---|---|---|---|---|---|---|
| 0 | 0 | 0 | 1.0000 | 0 | −0.0030 | 0 | 0 |
| 0 | 0 | 0 | 0.0002 | 0.9978 | 0.0661 | 0 | 0 |
| 0 | 0 | 0 | 0.0030 | −0.0661 | 0.9978 | 0 | 0 |
| 0 | 0 | 0 | −0.0082 | −0.0003 | −0.0022 | 0.0019 | −9.3921 |
| 0 | 0 | 0 | 0.0003 | −0.0302 | −0.0009 | 9.3921 | 0 |
| 0 | 0 | 0 | −0.0045 | −0.0011 | −0.6957 | 0.5895 | 0.0267 |
| 0 | 0 | 0 | 0 | 0 | 0 | 0 | 0 |
| 0 | 0 | 0 | 0 | 0 | 0 | 0 | 0 |
| 0 | 0 | 0 | 0 | 0 | 0 | 0 | 0 |
| 0 | 0 | 0 | 0.0786 | −0.6460 | −0.0727 | 0 | 0 |
| 0 | 0 | 0 | 0.4191 | 0.2050 | 0.0135 | 0 | 0 |
| 0 | 0 | 0 | 0.0138 | 1.1066 | −0.1634 | 0 | 0 |
| 0 | 0 | 0 | 0 | 0 | 0 | 0 | 0 |
| 0 | 0 | 0 | 0 | 0 | 0 | 0 | 0 |
| 0 | 0 | 0 | 0.0087 | 2.5346 | 0.7720 | 0 | 0 |
| 0 | 0 | 0 | 0 | 0 | 0 | 0 | 0 |
| 0 | 0 | 0 | 0.0149 | 0.0035 | 2.2985 | 0 | 0 |
| 0 | 0 | 0 | 0 | −2.3102 | 0 | 0 | 0 |

Columns 9 thru 13

| | | | | |
|---|---|---|---|---|
| 0 | 0 | 0 | 0 | 0 |
| 0 | 0 | 0 | 0 | 0 |
| 0 | 0 | 0 | 0 | 0 |
| 0 | 0.0285 | 0.2703 | 0 | −6.2479 |
| 0 | −0.2703 | 0.0285 | 0.0183 | −1.9881 |
| 0 | 0.0002 | −0.0008 | 0 | 0.0201 |
| 0 | 1.0000 | 0 | −0.0030 | 0 |
| 0 | 0.0002 | 1 | 0.0663 | 0 |
| 0 | 0.0030 | 0 | 1.0022 | 0 |
| 0 | −34.5087 | 2.4445 | −0.3293 | −225.5954 |
| 0 | −0.9768 | −13.8676 | −0.1437 | 322.9455 |
| 0 | −6.0511 | 0.4293 | −1.0703 | −39.5738 |
| 0 | 0.0222 | −1 | 0 | −3.6210 |
| 0 | −1 | −0.0222 | 0 | 0 |
| 0 | −3.7878 | 0.2649 | −2.1987 | −24.6825 |
| 0 | 0 | 0 | 0 | 0 |
| 0 | 0 | 0 | 0 | 0 |
| 0 | 0 | 0 | 1.9174 | 0 |

Columns 14 thru 18 (B1)

| | | | | |
|---|---|---|---|---|
| 0 | 0 | 0 | 0 | 0 |
| 0 | 0 | 0 | 0 | 0 |
| 0 | 0 | 0 | 0 | 0 |
| −1.9881 | 0 | 0 | 0.0047 | 0 |
| 6.2479 | 0 | 0 | 0.0019 | −0.0754 |
| −0.0017 | 0 | 0 | 1.4720 | 0 |
| 0 | 0 | 0 | 0 | 0 |
| 0 | 0 | 0 | 0 | 0 |
| 0 | 0 | 0 | 0 | 0 |
| 803.5631 | −0.4324 | 2.3433 | 0.1828 | 0.8278 |
| 90.5263 | 0.0070 | −0.0381 | −0.0278 | 0.1159 |
| 140.9024 | −1.2646 | 6.8524 | 0.4269 | 2.8635 |
| 0 | 0 | 0 | 0 | 0 |
| −3.6210 | 0 | 0 | 0 | 0 |
| 88.2189 | −4.9106 | 26.6092 | −2.0243 | 3.0450 |
| 0 | −0.3504 | 0 | 0 | 0 |
| 0 | 0 | 0 | −11.5302 | 0 |
| 0 | 0 | 0 | 0 | −17.9098 |

**B** =

| | | | |
|---|---|---|---|
| 0 | 0 | 0 | 0 |
| 0 | 0 | 0 | 0 |
| 0 | 0 | 0 | 0 |
| −0.7665 | −2.4089 | 0.3659 | 0 |
| 2.4089 | −0.7665 | 0.1509 | 3.7181 |
| −0.0006 | 0.0077 | 115.7010 | 0 |
| 0 | 0 | 0 | 0 |
| 0 | 0 | 0 | 0 |
| 0 | 0 | 0 | 0 |
| 309.8124 | −86.9780 | −19.9374 | −43.6758 |
| 34.9023 | 124.5111 | −3.0944 | −8.2959 |
| 54.3247 | −15.2576 | −62.6427 | −149.5450 |
| 0 | 4.1619 | 0 | 0 |
| 4.1619 | 0 | 0 | 0 |
| 34.0126 | −9.5163 | 304.0177 | −182.7158 |
| 0 | 0 | 0 | 0 |
| 0 | 0 | −382.2755 | 0 |
| 0 | 0 | 0 | 389.8808 |

(B2)

Typical values of the state and input vectors for scaling are

$$\hat{x} = (1 \quad 1 \quad 1 \quad 0.5 \quad 0.5 \quad 0.5 \quad 0.3 \quad 0.3 \quad 1 \quad 2 \quad 2 \quad 4 \quad 0.15 \quad 0.15 \quad 5 \quad 8 \quad 2 \quad 2)^T \tag{B3a}$$

$$\hat{u} = (0.09 \quad 0.09 \quad 0.09 \quad 0.3)^T \tag{B3b}$$

For the measurement and the output vector, respectively,

$$\hat{y} = (1 \quad 1 \quad 1 \quad 0.3 \quad 0.3 \quad 1)^T$$
$$\hat{z} = (1 \quad 1 \quad 1 \quad 1)^T \tag{B4}$$

follows.

## Appendix C: Design Parameters of the Model-Based Controllers

### LQG/LTR Controller

With the following definitions for the regulator

$$u(t) = \mathbf{G}x(t) \tag{C1}$$

with

$$\mathbf{G} = (\rho \mathbf{R}_1)^{-1} \mathbf{B}^T \mathbf{K} \tag{C2}$$

and

$$\mathbf{A}^T\mathbf{K} + \mathbf{K}\mathbf{A} - \mathbf{K}\mathbf{B}(\rho \mathbf{R}_1)^{-1}\mathbf{B}^T\mathbf{K} + \mathbf{C}^T\mathbf{Q}_y\mathbf{C} = 0 \tag{C3}$$

and the estimator

$$\dot{z}(t) = [\mathbf{A} - \mathbf{H}\mathbf{C}]z(t) + \mathbf{H}w(t) \tag{C4}$$

with

$$\mathbf{H} = \Sigma \mathbf{C}^T (\mu \Theta_1)^{-1} \tag{C5}$$

and

$$\mathbf{A}\Sigma + \Sigma \mathbf{A}^T - \Sigma \mathbf{C}^T (\mu \Theta_1)^{-1} \mathbf{C} \Sigma + \mathbf{B} \Xi \mathbf{B}^T = 0 \tag{C6}$$

the design parameters are: $\rho$, $\mathbf{R}_1$, $\mathbf{Q}_y$, $\mu$, $\Theta_1$, $\Xi$. The latter two are chosen as identity matrices of appropriate size in all designs.

The LQG/LTR design for the first subsystem (Section V.C.1) is accomplished with

$$\mathbf{C}_y = \text{diag}(1 \quad 0.8) \tag{C7}$$

$$\mathbf{R}_1 = \mathbf{I}_2$$

$$\rho = 0.18$$

$$\mu = 10^{-4}$$

For the second subsystem (Section V.C.2.) the following design is used:

$$\mathbf{Q}_y = \text{diag}(1 \quad 1 \quad 0.3 \quad 0.3), \quad \mathbf{R}_1 = I_2$$

$$\rho = 0.03 \tag{C8}$$

$$\mu = 10^{-4}$$

**Modal Controller**

The modal design as in Lohmann,[11] Section 3, is used for the first subsystem. The controller is defined by the set of desired eigenvalues for each path and the value $\mu$ for the LTR observer.

$$\boldsymbol{ev}_1 = (-4.3769 \pm 1.6532j \quad -24.9986 \pm 17.6756j)^T \tag{C9a}$$

$$\boldsymbol{ev}_2 = (-9.4566 \pm 3.3800j \quad -24.9777 \pm 17.6549j)^T \tag{C9b}$$

$$\boldsymbol{ev}_{\text{zero comp}} = (-1.6045 \pm 1.8586 \quad -10.6010 \quad -6.66667)^T \tag{C9c}$$

$$\mu = 10^{-4} \tag{C9d}$$

For the second subsystem the approach in Lohmann,[11] Section 7.2, is used. Again, the eigenvalues for each path and the value $\mu$ for the LTR step define the controller:

$$\boldsymbol{ev}_1 = (-1.4890 \pm 1.6734j \quad -9.0598 \pm 18.6846j \quad -25.0140 \pm 17.5656j \quad -4.0757 \quad -30.0)^T \tag{C10a}$$

$$\boldsymbol{ev}_1 = (-1.4862 \pm 1.6666j \quad -25.5250 \pm 17.2551j \quad -19.1822 \pm 24.4183j \quad -4.5649 \quad -35.0)^T \tag{C10b}$$

$$\boldsymbol{ev}_{\text{zero comp}} = (-14.4158 \quad -14.4157)^T \tag{C10c}$$

$$\mu = 10^{-4} \tag{C10d}$$

## References


[1] Clavel, R., "DELTA, A Fast Robot with Parallel Geometry," *Proceedings of the International Symposium on Industrial Robots*, Australian Robot Association, Inc., Vol. 19, 1988, pp. 91–100.

[2] Bramwell, A. R. S., *Helicopter Dynamics*, Edward Arnold, London, 1976.

[3] Johnson, W., *Helicopter Theory*, Princeton University Press, Princeton, NJ, 1980.

[4] Prouty, R. W., *Helicopter Performance, Stability, and Control*, Krieger, Malabar, FL, 1990.

[5] von Grünhagen, W., "Modellierung und Simulation von Hubschraubern, mathematische Beschreibung," DFVLR-Institutsbericht IB 111–88/06, Braunschweig, Germany, 1988.

[6] "Military Specification—Flying Qualities of Piloted Airplanes," Aeronautical Systems Division/ENESS, MIL-F-8785C, Wright-Patterson AFB, OH.

[7] "Aeronautical Design Standard, Handling Qualities Requirements for Military Rotorcraft," U.S. Army Aviation Systems Command, ADS-33C, Washington, DC, Aug. 1989.

[8] Eckblad, M., "Reduced-Order Modeling and Controller Design for a High-Performance Helicopter," *Journal of Guidance, Control, and Dynamics*, Vol. 13, No. 3, 1990, pp. 439–449.

[9] Garrard, W. L., Low, E., and Prouty, S., "Design of Attitude and Rate Command Systems for Helicopters Using Eigenstructure Assignment," *Journal of Guidance, Control, and Dynamics*, Vol. 12, No. 6, 1989, pp. 783–791.

[10] Apkarian, P. R., "Structured Stability Robustness Improvement by Eigenspace Techniques: A Hybrid Methodology," *Journal of Guidance, Control, and Dynamics*, Vol. 12, No. 2, 1989, pp. 162–168.

[11] Lohmann, B., *Vollständige und teilweise Führungsentkoppelung im Zustandsraum*, Diss., Fortschritts-Berichte VDI-Verlag, Reihe 8, No. 244, Karlsruhe, Germany, 1991.

[12] Freudenberg, J. S., and Looze, D. P., "Right Half Plane Poles and Zeros and Design Tradeoffs in Feedback Systems," *IEEE Transactions on Automatic Control*, Vol. AC-30, No. 6, 1985, pp. 555–565.